The Temperature Effects on the Coherent Structures Induced by the Modulational Instability in Photovoltaic Photorefractive Crystal Circuit

Woo-Pyo Hong

Department of Electronics Engineering, Catholic University of Daegu, Hayang, Gyongsan, Gyungbuk 712-702, South Korea

Reprint requests to E. H.; E-mail: wphong@cu.ac.kr

Z. Naturforsch. **64a,** 729 – 738 (2009); received August 12, 2008 / March 2, 2009

The temperature effects on the modulational instability of broad optical beams in a photovoltaic photorefractive crystal circuit has been investigated. The analytic gain formula for the modulational instability has been obtained by applying a linear stability analysis. Non-zero gain of the modulational instability is shown to exist both for positive and negative photovoltaic fields for a wide range of modulational instability frequency. The evolutions of the initial broad beam under the modulational instability are numerically investigated for the $BaTiO_3$ crystal as a photovoltaic photorefractive medium with a positive photovoltaic field by varying the crystal temperatures. Some symmetric and asymmetric solitary-waves and periodic waves have been shown to exist as results of mutual interactions between the localized beams induced by the modulational instability. Their dynamical behaviour and mutual interaction are sensitive to the variation of crystal temperature.

Key words: Spatial Soliton; Photovoltaic Photorefractive Crystal Circuit; Modulational Instability; Temperature Effect; Numerical Simulation.

PACS numbers: 42.65.Tg, 42.81Dp, 42.65Sf

1. Introduction

Optical solitons are self-trapped and self-guided solitary waves that propagate forward while maintaining their shape as a real particle [1 – 5]. The discovery of photorefractive spatial solitons [6 – 8] has given an enormous boost to investigations of optical soliton physics. Earlier, solitons were investigated mostly in materials possessing a Kerr nonlinearity. In these media, the existence of fundamental spatial solitons was predicted and observed, and these solitons were stable in one dimension only. They were found to collapse in two and three spatial dimensions. Photorefractive (PR) media show saturation in their nonlinearity, which suppresses the collapse of solitons in two and three dimensions. In addition to their stability in more than one dimension and, thus, their ability to induce waveguides, they possess various other desirable properties. PR spatial solitons need very low optical power (microwatt) for their formation. The response of PR media is wavelength sensitive, so PR spatial solitons can be generated with microwatts power and the waveguide induced by them can be employed to guide high power beams for which the PR medium is less sensitive. The waveguides induced by PR solitons can be permanently impressed and can be erased and overwritten. Soliton induced waveguides can be used for steering and controlling other beams, which can find applications in direction couplers, beam splitters, nonlinear frequency conversion, etc. So far, three different types of steady-state photorefractive solitons have been predicted. The one, which was identified first, is the screening soliton. Both bright and dark screening solitons (SS) in the steady state are possible when an external bias voltage is applied to a non-photovoltaic photorefractive crystal [6, 7]. The second kind is the photovoltaic soliton [9 – 11], the formation of which, however, requires an unbiased PR crystal that exhibits the photovoltaic effect, i.e., the generation of a dc current in a medium illuminated by a light beam. Recently, a third kind of photorefractive soliton has been introduced [12 – 15], which arises when an electric field is applied to a photovoltaic photorefractive crystal. These solitons owe their existence to both the photovoltaic effect and spatially non-uniform screening of the applied field and are known as screening photovoltaic solitons (SP).

An important phenomenon, in connection with the formation of spatial solitons in photovoltaic photorefractive media, is the modulational instability (MI), which is inherent in most nonlinear systems and occurs

0932–0784 / 09 / 1100–0729 $ 06.00

as a result of interplay between the nonlinearity and the dispersion in temporal domain and between the nonlinearity and the diffraction in the spatial domain [16 – 19]. As a result continuous wave (CW) or quasi-CW radiation propagating in a nonlinear dissipative medium may suffer an instability with respect to weak periodic transverse modulation of the steady state, resulting in a break up of CW into a train of short pulses. In the spatial domain, for a narrow beam, self phase modulation exactly balances the diffraction, and robust spatial solitons are obtained while a broad optical beam disintegrates into many filaments during propagation in the same self-focusing nonlinear medium. For a broad beam, complete balance of diffraction is not achieved due to some internal, or maybe external noise, and the same focusing nonlinearity leads to transverse instability and the formation of multiple filaments of the beam. It occurs in the same parameter space where bright solitons form and it is considered to be as a precursor of soliton formation. Consequently, it would be of interest to know if a dynamical spatial soliton can exhibit modulational instability.

Recently, Zhang et al. [20] have investigated the temperature effects on the evolution and stability of a separate photovoltaic bright/dark soliton pair formed in a serial photovoltaic photorefractive crystal circuit. It has been known that the photorefractive effects are dependent on the dark irradiance of the crystal, which is also dependent on the temperature [21]. They have shown by numerical simulations that adjusting each crystal temperature can affect the dynamical evolution of the soliton formed in the other crystal. The crystal temperature regime for the bright soliton and dark solitons have been identified by the authors [20]. More recently, Guangyonga et al. [22] have studied the temperature effects on the bending of the dynamical evolutions of the analytic solitary waves. In this paper, we investigate how the temperature of one crystal affects the formation and propagation of coherent structures induced by the perturbed CW states under the MI for both crystals in a photovoltaic photorefractive crystal circuit.

The paper is organized as follow. In Section 2, we obtain the analytic expression for the gain spectrum and find the MI gain dependence on the photovoltaic field and the temperature of the crystals. In Section 3, we numerically investigate the effects of temperature on the evolutions of the spatial solitons induced by the initial steady beam under weak modulational field. In particular, we show that symmetric and asymmetric solitary-waves and periodic waves exist as results of mutual interactions between the localized beams induced by the MI and their dynamical behaviour and mutual interaction are sensitive to the variation of crystal temperature. The results of this work are briefly summarized in Section 4.

2. Gain by the Modulations Instability

To study the modulational instability in a photovoltaic photorefractive circuit system, we consider two $BaTiO_3$ crystals, denoted by P and $\hat{P}$, as the components for such a system, where an optical beam propagates along the crystal z-axis and is permitted to diffract only along the x-direction with different optical c-axis (see [20] for details). By defining the dimensionless envelopes of the optical beams propagating the crystals as $U = \sqrt{(}I/I_\mathrm{d})$ and $\hat{U} = \sqrt{(}\hat{I}/\hat{I}_\mathrm{d})$, respectively, where I_d and $\hat{I}_\mathrm{d}$ are the irradiance and I and $\hat{I}$ are the intensities of the beams. Zhang et al. [20, 22] have obtained the following beam envelope evolution equations:

$$\begin{aligned} \mathrm{i}U_\xi + \frac{1}{2}U_{ss} - \alpha\frac{(\rho - |U|^2)}{1+|U|^2} - \beta(\rho+1)\frac{U}{1+|U|^2} = 0, \\ \mathrm{i}\hat{U}_\xi + \frac{1}{2}\hat{U}_{ss} - \hat{\alpha}\frac{(\hat{\rho} - |\hat{U}|^2)}{1+|\hat{U}|^2} - \hat{\beta}(\hat{\rho}+1)\frac{\hat{U}}{1+|\hat{U}|^2} = 0, \end{aligned} \tag{1}$$

where $U_\xi = \partial U/\partial\xi$, $\xi = z/(kx_0^2)$, $U_{ss} = \partial^2 U/\partial s^2$, $s = z/x_0$, x_0 is an arbitrary spatial width of the crystal, $k = n_\mathrm{e}k_0 = (2\pi/\lambda_0)n_\mathrm{e}$, λ_0 is the free-space wavelength of the lightwave to be used, n_e is the unperturbed extraordinary index of refraction, $\alpha = \sigma E_\mathrm{p}$ and $\alpha = \hat{\sigma}\hat{E}_\mathrm{p}$, E_p and $\hat{E}_\mathrm{p}$ are the photovoltaic field constants, $\beta = -\sigma\Gamma E_\mathrm{p}$, $\hat{\beta} = -\hat{\sigma}\Gamma\hat{E}_\mathrm{p}$, $\Gamma = \hat{I}_\infty/(I_\mathrm{d}+\hat{I}_\mathrm{d}+I_\infty)$, $\rho = I_\infty/I_\mathrm{d}$, $I_\infty = I(x \longrightarrow \pm\infty, z)$, $\sigma = \hat{\sigma} = (k_0x_0)^2/(n_\mathrm{e}r_{33})$ and r_{33} is the electro-optic coefficient [20, 22].

The evolution equations in (1) are coupled to each other by the constants between β and $\hat{\beta}$, which are strongly related to the temperatures of crystals through the dark irradiance dependence on Γ [20, 21]

$$\begin{aligned} I_\mathrm{d} = I_{\mathrm{d}0}\left(\frac{T}{300}\right)^{3/2}\exp\left[\left(\frac{E_\mathrm{t}}{k_\mathrm{B}}\right)\left(\frac{1}{300}\right) - \left(\frac{1}{T}\right)\right], \\ \hat{I}_\mathrm{d} = \hat{I}_{\mathrm{d}0}\left(\frac{\hat{T}}{300}\right)^{3/2}\exp\left[\left(\frac{\hat{E}_\mathrm{t}}{k_\mathrm{B}}\right)\left(\frac{1}{300}\right) - \left(\frac{1}{\hat{T}}\right)\right], \end{aligned} \tag{2}$$

where $I_{\mathrm{d}0}$ and $\hat{I}_{\mathrm{d}0}$ are the values of the dark irradiance at 300 K, respectively, E_t and $\hat{E}_t$ are the level locations

in the gap of crystal, k_B is Boltzmann's constant, and T and $\hat{T}$ are the absolute temperature. In the following analysis, we take $E_t = \hat{E}_t = 10^{-19}J$ for the $BaTiO_3$ crystal [20].

In order to investigate how weak perturbations evolve along the beam evolution distance, we consider the following linear instability analysis. The steady-state solution of (1) is given by

$$U = Re^{i\psi(\xi)}, \quad \hat{U} = Qe^{i\phi(\xi)}, \tag{3}$$

where R and Q are the dimensionless powers of the optical waves and the phase shift $\psi(\xi)$ and $\phi(\xi)$ are related to R and Q, respectively, and the evolution distance ξ through

$$\psi(\xi) = \frac{[(-\alpha-\beta)\rho + \alpha R^2 - \beta]\xi}{1+R^2}, \quad \phi(\xi) = \frac{\left[\left(-\hat{\alpha}-\hat{\beta}\right)\hat{\rho} + \hat{\alpha}Q^2 - \hat{\beta}\right]\xi}{1+Q^2}. \tag{4}$$

The instability of the steady state can be examined by employing a perturbation in the steady-state solutions of the form

$$\begin{aligned} U(\xi,s) &= [R + \kappa(\xi,s)]\exp\left[\frac{((-\alpha-\beta)\rho + \alpha R^2 - \beta)\xi}{1+R^2}\right], \\ \hat{U}(\xi,s) &= [Q + \eta(\xi,s)]\exp\left[\frac{((-\hat{\alpha}-\hat{\beta})\hat{\rho} + \hat{\alpha}Q^2 - \hat{\beta})\xi}{1+Q^2}\right], \end{aligned} \tag{5}$$

where the complex field satisfy $|\kappa(\xi,s)| \ll R$ and $|\eta(\xi,s)| \ll Q$. Thus, if the perturbed field grows exponentially, the steady states become unstable. By substituting (5) into (1) and collecting the terms linear in κ and η, we obtain the linearized equations as

$$\begin{aligned} &2i(1+R^2)^2\kappa_\xi + (1+R^2)^2\kappa_{ss} + 2R^2(\rho+1)(\beta+\alpha)(\kappa+\kappa^*) = 0, \\ &2i(1+Q^2)^2\eta_\xi + (1+Q^2)^2\eta_{ss} + 2Q^2(\hat{\rho}+1)(\hat{\beta}+\hat{\alpha})(\eta+\eta^*) = 0, \end{aligned} \tag{6}$$

where * denotes complex conjugates. We assume general solutions of the form

$$\eta(\xi,s) = a_1 e^{i(K\xi-\Omega s)} + a_2 e^{-i(K\xi-\Omega s)}, \quad \kappa(\xi,s) = a_3 e^{i(K\xi-\Omega s)} + a_4 e^{-i(K\xi-\Omega s)}, \tag{7}$$

where K and Ω represent the wave number and the shifted frequency, respectively, and a_i is the amplitude of the perturbation field. To find the dispersion relation between K and Ω, we require

$$\begin{bmatrix} -\Lambda_1 K^2 + 4\Lambda_2 R^2 & 2\Omega\Lambda_1 & 0 & 0 \\ -2i\Lambda_1\Omega & i\Lambda_1 K^2 & 0 & 0 \\ 0 & 0 & -\Lambda_3 K^2 + 4\Lambda_4 Q^2 & 2\Omega\Lambda_3 \\ 0 & 0 & -2i\Lambda_3\Omega & i\Lambda_3 K^2 \end{bmatrix} = 0, \tag{8}$$

where

$$\begin{aligned} &\Lambda_1 = (1+R^2)^2, \quad \Lambda_2 = (\rho+1)(\alpha+\beta), \\ &\Lambda_3 = (1+Q^2)^2, \quad \Lambda_4 = (\hat{\rho}+1)(\hat{\alpha}+\hat{\beta}). \end{aligned} \tag{9}$$

From (6) and (8), it seems that the dispersion relations for both crystals are completely independent to each other, from which we obtain only two solutions with a purely complex value, i. e.,

$$\begin{aligned} K &= \frac{\sqrt{2\Lambda_1(\Lambda_2 R^2 - \sqrt{{\Lambda_2}^2 R^4 + {\Lambda_1}^2\Omega^2})}}{\Lambda_1}, \\ \hat{K} &= \frac{\sqrt{2\Lambda_3(\Lambda_4 Q^2 - \sqrt{{\Lambda_4}^2 Q^4 + \Omega^2{\Lambda_3}^2})}}{\Lambda_3}. \end{aligned} \tag{10}$$

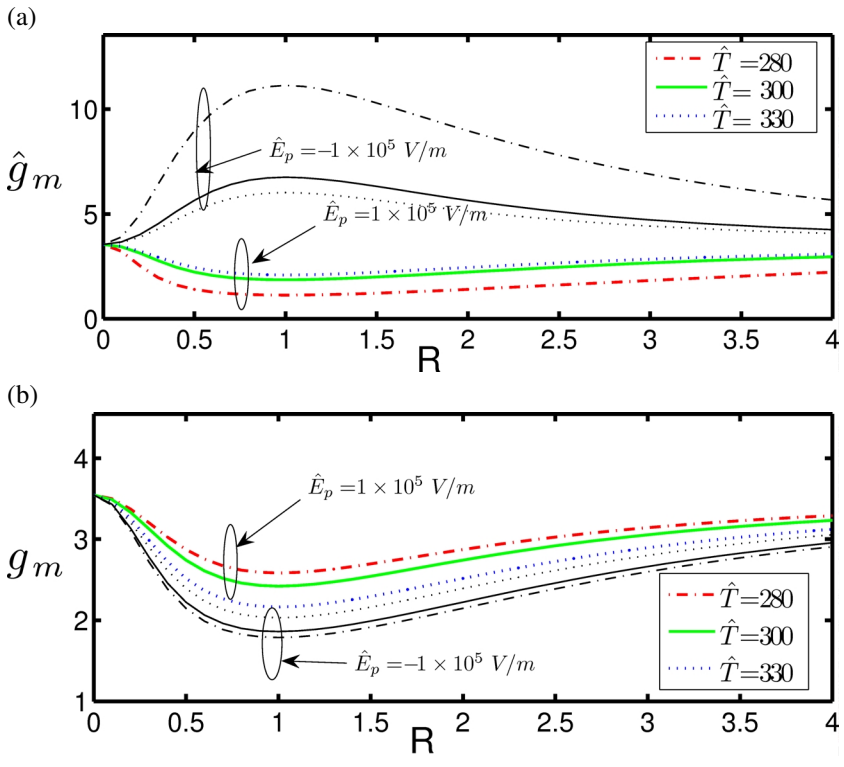

Fig. 1. Plots of the maximum gains $\hat{g}_{\rm m}$ and $g_{\rm m}$ for crystal $\hat{P}$ and R, respectively, as function of the power for two $\hat{E}_{\rm p}$ values with increasing $\hat{T}$. (a) The maximum gain for the case of $\hat{E}_{\rm p} = -1\cdot 10^5$ V/m is larger than that of $\hat{E}_{\rm p} = 1\cdot 10^5$ V/m, regardless of the values of $\hat{T}$. The maximum gain peak occurs at the power $R \approx 1$, regardless of the sign of $\hat{E}_{\rm p}$, and it gradually decreases with increasing the power R. (b) The gain for the case of $\hat{E}_{\rm p} = 1\cdot 10^5$ V/m is larger than that of $\hat{E}_{\rm p} = -1\cdot 10^5$ V/m, regardless of $\hat{T}$. The minimum of $g_{\rm m}$ occurs at $R \approx 1$ and its values gradually increasing with increasing the power R.

Thus, we find that the square bracket of the wave number K and $\hat{K}$ are always negative for $\Omega \neq 0$ regardless of the values of the crystal parameters. In such a medium, a perturbation grows exponentially with ξ for any frequencies other than $\Omega = 0$, leading to an instability in the steady-state beam. This instability is referred to as the MI which leads to spontaneous break up of the steady-state beam into several filaments or coherent structures.

We plotted in Figures 1a and b the maximum MI gains of both crystals, defined as $g_{\rm m}(\Omega) = 2|{\rm Im}(K)|$ and $\hat{g}_{\rm m} = 2|{\rm Im}(\hat{K})|$, respectively, as functions of the power by assuming $R = Q$ and the temperature $\hat{T}$ of the crystal $\hat{P}$ for the modulation frequency in the range of $|\Omega| \leq 2\pi$ for the cases of $\hat{E}_{\rm p} = 1\cdot 10^5$ V/m and $\hat{E}_{\rm p} = -1\cdot 10^5$ V/m, respectively, with a set of the crystal parameters: $T = 300$ K, $E_{\rm p} = 1\cdot 10^5$ V/m, $\lambda_0 = \hat{\lambda}_0 = 0.5\ \mu$ m, $n_{\rm e} = \hat{n}_{\rm e} = 2.365$, $r_{33} = \hat{r}_{33} = 80\cdot 10^{-12}$ mV^{-1}, and $x_0 = \hat{x}_0 = 40\ \mu$m. It is shown in Figure 1a that $\hat{g}_{\rm m}$ for the case of $\hat{E}_{\rm p} = -1\cdot 10^5$ V/m is larger than that of $\hat{E}_{\rm p} = 1\cdot 10^5$ V/m, regardless of the values of $\hat{T}$, but decreases as both $\hat{T}$ and R increase. However, for the case of $\hat{E}_{\rm p} = -1\cdot 10^5$ V/m, $\hat{g}_{\rm m}$ increases with both increasing $\hat{T}$ and the power R. The gain for the case of $\hat{E}_{\rm p} = 1\cdot 10^5$ V/m in Figure 1b is larger than that of $\hat{E}_{\rm p} = -1\cdot 10^5$ V/m, regardless of $\hat{T}$. The minimum of $g_{\rm m}$ also occurs at $R \approx 1$ and its values gradually increasing with increasing R. Even though we do not show here, for the case of $R \neq Q$, the maximum gain curves show the similar characteristics as those in Figures 1a and b.

In the above gain calculations, we used $I_{\rm d} = I_{\rm d0} = \hat{I}_{\rm d0}$ (since the temperature of crystal P is fixed at $T = 300$ K) and the initial beam parameters $I_0 = I_{\rm d}$, $I_\infty = 0$, $\hat{I}_\infty = \hat{I}_{\rm d}$ (or $\hat{\rho} = 1$). The reason for the MI gains having different characteristic dependence on the power R, $\hat{E}_{\rm p}$, and $\hat{T}$, in spite of seeming completely independent dispersion relations in (10), is due to the functional relation between the parameters β and $\hat{T}$ as $\beta = -\rho/(1+\hat{\rho}+\phi)\sigma\hat{E}_{\rm p}$, where $\phi = (\hat{T}/300)^{-3/2}\exp[-\hat{E}_{\rm t}/k_B(1/300 - 1/\hat{T})]$. Needless to say, there is also similar functional relation between $\hat{\beta}$ and T. Thus, as demonstrated in Figures 1a and b, the maximum MI gain for each crystal is different for the same temperatures. Since the system is always unstable for a wide range of the system parameters, we may expect that the MI applied to weakly perturbed initial

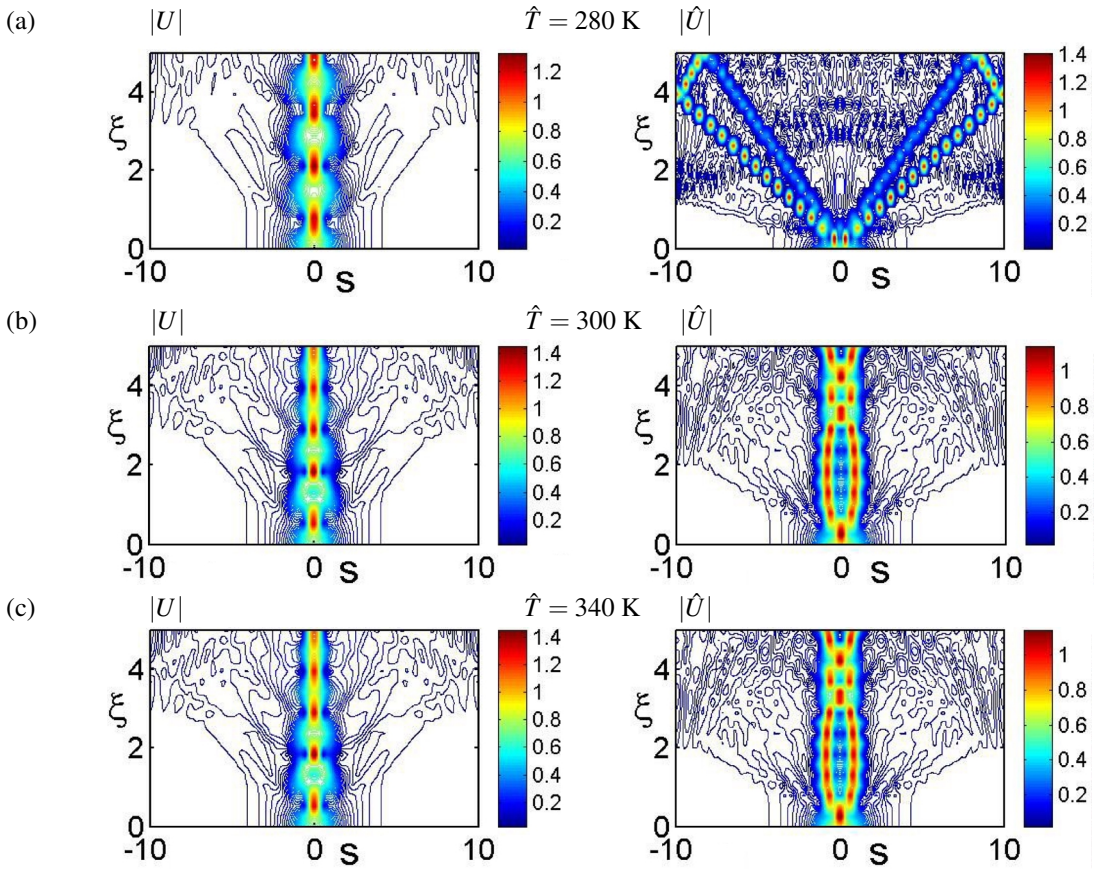

Fig. 2. Numerical evolutions of the localized initial beam in the form of $U(0,s) = \varepsilon_{\mathrm{m}} \operatorname{sech}(s)$, where $\varepsilon_{\mathrm{m}} = 0.5$ with increasing $\hat{T}$. Left pane (a) – (c): The contour plots of $|U|$ show the transformation of the initial localized beam to a breather with breathing periodicity decreasing as $\hat{T}$ increases. Right pane (a) – (c): The contour plots of $|\hat{U}|$ show more diverse evolution characteristics. (a) The initial beam splitting into two beams propagating to the left and right directions. (b) Attractive interaction between the splitted beams occurs at $\xi \approx 3$. (c) Stable bright soliton propagation appears $\xi \geq 3$ after showing pulsating transient propagation.

CWs bring out interesting dynamics during their evolutions.

3. Temperature Effects on the Solitons Induced by Modulational Instability

In order to understand the evolution of broad optical beam propagation under the MI for the coupled $BaTiO_3$ crystals with varying temperatures, we solve (1) by utilizing the split-step Fourier method under periodic boundary condition [23]. Before considering the MI process in the crystal, we first investigate the evolution of a localized initial beam in the form of $U(0,s) = \varepsilon_{\mathrm{m}} \operatorname{sech}(s)$, where $\varepsilon_{\mathrm{m}} = 0.5$, by varying the temperature of the crystal $\hat{P}$ from $\hat{T} = 280$ K up to $\hat{T} = 340$ K. The localized initial beam may be considered as a perturbation to the exact bright solitary wave found in [20]. This may help us to understand the evolutions of the transient localized beams to appear as a result of the perturbed CW states by the MI.

The crystal parameters used for the simulation are the same as those in Figure 1a with $E_{\mathrm{p}} = \hat{E}_p = 1 \cdot 10^5$ V/m and fixed temperature at $T = 300$ K for the crystal P. Figures 2a – c show the evolutions of $|U|$ and $|\hat{U}|$ in contour plots, respectively, with increasing $\hat{T}$. The evolutions of $|U|$ in the left pane of Figures 2a – c show periodically breathing solitons (breathers) along the propagation distance and the breathing periodicity increases with increasing $\hat{T}$, while the propagation of the exact stationary solution (bright soliton) as initial input beam has been shown to maintain a good stabil-

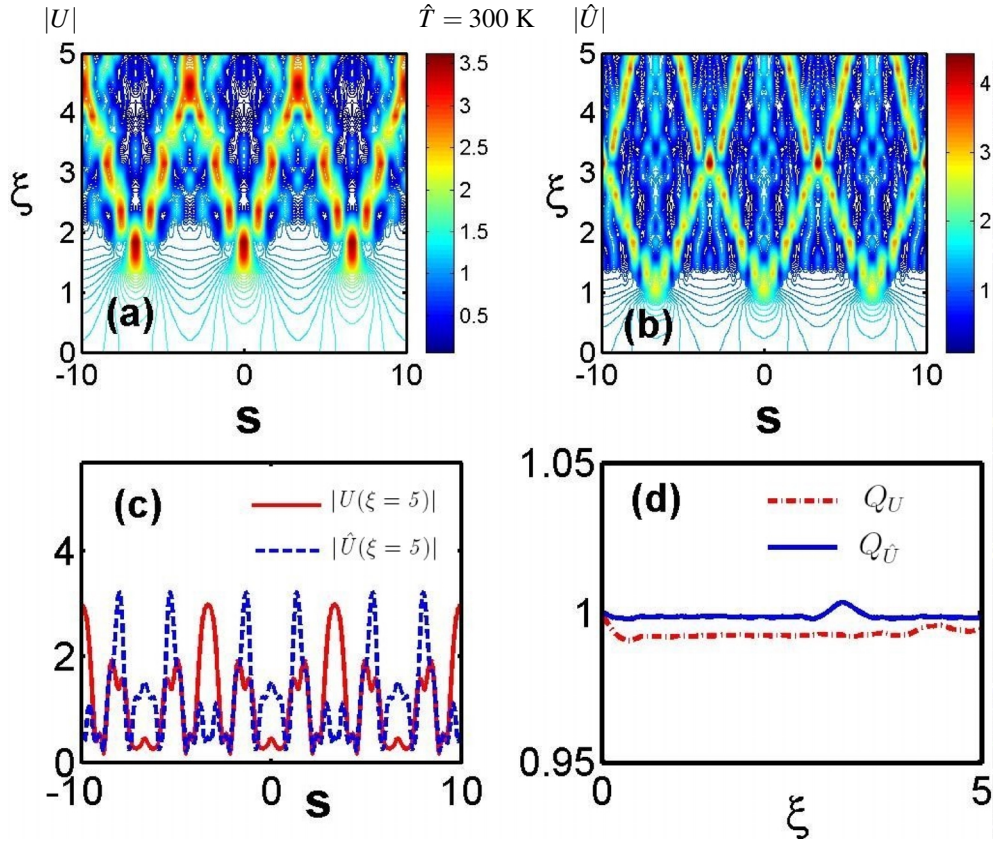

Fig. 3. Evolutions of the perturbed CW states by the MI for fixed crystal temperatures. (a) Evolution of $|U|$ shows three localized beams at $\xi \approx 1.8$, which subsequently split into two localized beams or filaments. Interaction between the filaments at $\xi \approx 3$ to form larger localized beams at $\xi \approx 4.5$. (b) Evolution of $|\hat{U}|$ shows stronger elastic interaction at $\xi \approx 3.2$. (c) The snapshots of $|U|$ and $|\hat{U}|$ at $\xi = 5.0$. Both symmetric and asymmetric localized beams with side wings for U and $\hat{U}$ appear. (d) Both the evolutions of Q_U and $Q_{\hat{U}}$ show less than 1% deviation from the initial values, implying stability of the MI processes.

ity during its evolution for increasing temperatures in [20]. On the other hand, the temperature effect on the evolution of $|\hat{U}|$ results in more diverse characteristics as demonstrated in the right pane of Figures 3a – c; the initial beam splits into two beams propagating into the right and left direction, still maintaining breather-like behaviour, as shown in Figure 2a for $\hat{T} = 280$ K; attractive interaction between the splitted beams occurs at $\xi \approx 3$ in Figure 2b for $\hat{T} = 300$ K; stable bright soliton propagation appears $\xi \geq 3$ after showing pulsating transient propagation as depicted in Figure 2c for $\hat{T} = 340$ K. These results indicate that the evolution of optical beam in the crystal is very sensitive both the shape and the magnitude of the initial beam, and the temperature of the crystal strongly affects the evolution characteristics of both beams in the crystal circuit. Thus, we expect to observe more complicated evolutionary patterns by the MI induced localized beams since one can introduce a few localized beams from the perturbed CW states, depending on the strength of modulation frequency.

To investigate the evolution of perturbed CW state by the MI with varying crystal temperatures, we consider sinusoidally-modulated CW beam in the form of

$$\begin{aligned} U(0,s) &= R_0 + \varepsilon_{\mathrm{m}} \sin(\Omega_{\mathrm{m}} s), \\ \hat{U}(0,s) &= Q_0 + \varepsilon_{\mathrm{m}} \sin(\hat{\Omega}_{\mathrm{m}} s), \end{aligned} \tag{11}$$

where ε_{m} is the normalized modulation amplitude and Ω_{m} and $\hat{\Omega}_{\mathrm{m}}$ are the angular frequencies which can be determined from the above gain spectra when the model parameters are fixed.

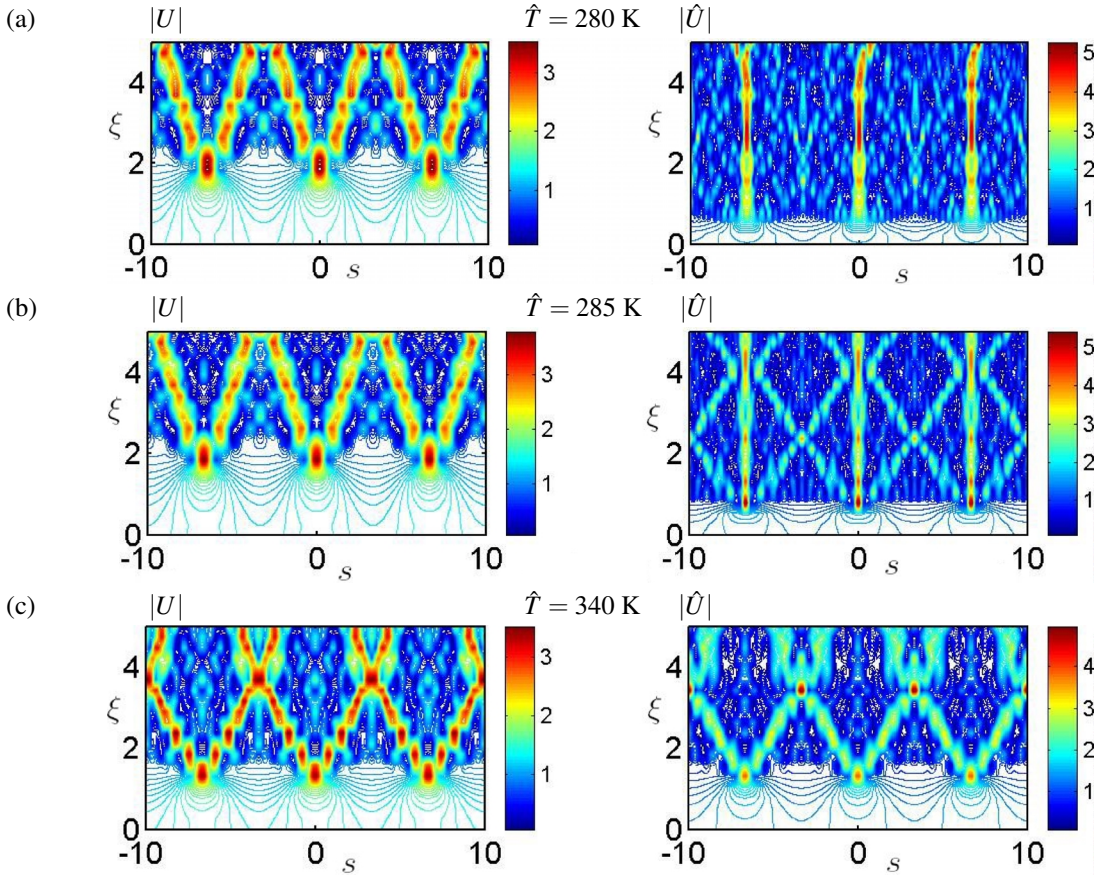

Fig. 4. Evolutions of $|U|$ and $|\hat{U}|$ with increasing $\hat{T}$. Left pane: (a) and (b) Attractions between the splitted beams are both shown with similar evolution patterns; (c) Stable breathers collide to form a periodic wave. Right pane: (a) For the case of $\hat{T} = 280$ K, solitary-wave propagation is shown between $2.5 \leq \xi \leq 3.5$; (b) Complicated interaction pattern between the breather and solitary wave appears; (c) The evolution of $|\hat{U}|$ is similar to that of $|U|$.

The result of the evolution of the perturbed CW states by the MI is presented in Figure 3 by choosing $R_0 = Q_0 = 1$, $\varepsilon_m = 0.05R_0 = 0.05Q_0$, and $\Omega_m = \hat{\Omega}_m = 0.1$ with the same set of the crystal parameters used in Figure 2 and setting $T = \hat{T} = 300$. It is found in Figure 3a that the modulated initial CW state of U transforms into three localized beams at $\xi \approx 1.8$, which subsequently split into two localized beams or filaments. It is interesting to note that the filamented beams attract each other, for example, at $\xi \approx 3$, before transforming into larger localized beams at $\xi \approx 4.5$. On the other hand, Figure 2b shows the evolution of $\hat{U}$ with qualitatively similar evolution pattern as that of U. However, it is different in the sense that the splitted beams undergo more stronger elastic type interaction at $\xi \approx 3.2$. The snapshots of $|U|$ and $|\hat{U}|$ at $\xi = 5.0$ are plotted in Figure 3c, respectively. It is interesting to note that symmetric and asymmetric localized beams with side wings at both U and $\hat{U}$, respectively, appear. We thus name them as the two coherent structures as symmetric solitary and asymmetric solitary waves, respectively. We now check the stability of the MI process by calculating the total energy defined as $\mathcal{E}(\xi) \equiv \int_{-\infty}^{\infty} |U(\xi, s)|^2 ds$ and plotting $Q(\xi) \equiv \mathcal{E}(\xi)/\mathcal{E}(0)$ in Figure 3c. According to the plots, both the evolutions of Q_U and $Q_{\hat{U}}$ show a minor deviation, i. e., less than 1% of the initial value, implying a stability of the MI processes (note the scale of plot in Figure 3c) and the energy conservation during the MI process. In particular, $Q_{\hat{U}}$ shows no deviation from its initial value except at $\xi = 3.2$ where a slight increase in $Q_{\hat{U}}$ occurs due to the 'almost elastic' collision between

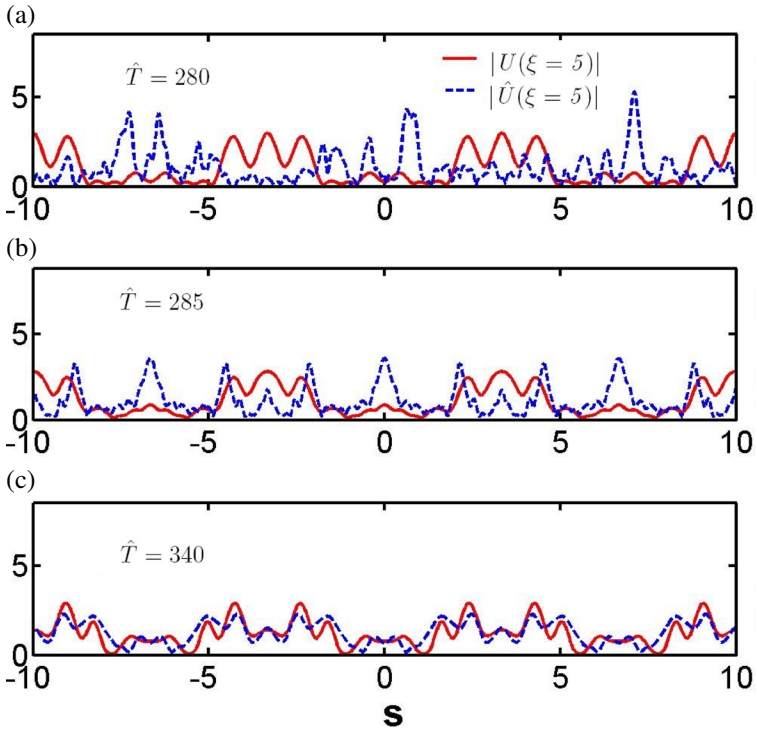

Fig. 5. The snapshots of $|U|$ and $|\hat{U}|$ at $\xi = 5.0$. (a) Highly periodic and symmetric waves with three peaks for $|U|$ show up, while irregular filamented beam appear for $|U|$. (b) and (c) Temperature increase results in highly symmetric waves structures for both $|\hat{U}|$ and $|U|$.

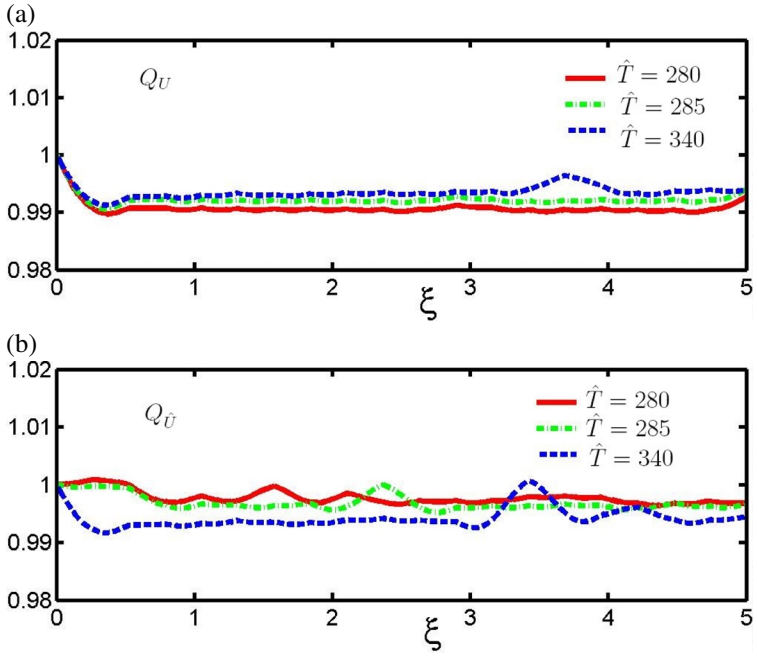

Fig. 6. Evolutions of $Q_U(\xi)$ and $Q_{\hat{U}}(\xi)$ corresponding to Figures 4a – c. For all cases the energy of both crystals show less than 1% deviation from the initial value. (a) For the case of Q_U at higher crystal temperature, the energy fluctuation is relatively less. (b) For the case of $\hat{Q}_U$ at lower crystal temperature, the energy fluctuation is relatively less.

the breathers, as shown in Figure 3b. The meaning of 'almost elastic' collision between the breathers is more clearly demonstrated by the fact that $Q_{\hat{U}}$ returns to 1.0.

Figures 4a – c show the evolutions of the initial perturbed beam by the MI for the same crystal parameters as Figure 3 for three different $\hat{T}$. The evolution pat-

terns of $|U|$ for the cases of $\hat{T} = 280$ K and $\hat{T} = 285$ K are very similar to each other, as depicted in the left pane of Figures 4a and b. However, for the case of $\hat{T} = 340$ K, we find a drastic change in the evolution of $|U|$ in the sense that stable breathers collide to form periodic waves, which are more clearly presented in the snapshots of Figure 5. On the other hand, the evolution of $|\hat{U}|$ for the case of $\hat{T} = 280$ K shows a solitary-wave propagation between $2.5 \leq \xi \leq 3.5$ in Figure 4a. A slight increase in the crystal temperature results in more complicated interaction pattern between the breather and solitary-wave, as shown in Figure 4b for $\hat{T} = 285$ K. For the case of $\hat{T} = 340$ K in Figure 4c, we find qualitatively similar evolution pattern of $|\hat{U}|$ as $|U|$.

The snapshots of $|U|$ and $|\hat{U}|$ at $\xi = 5.0$ in Figures 5a – c, respectively, show the dependence on $\hat{T}$ on the formation of periodic waves. Highly periodic and symmetric waves with multi peaks, similar to Figure 2c, for U and $\hat{U}$ appear regardless of the crystal temperatures, except at $\hat{T} = 280$ K where non-periodic filamented beams are observed for $\hat{U}$ as shown in Figure 5a.

Finally, we calculated the evolutions of the normalized energies, $Q_U(\xi)$ and $Q_{\hat{U}}(\xi)$, respectively, in Figures 6a and b, corresponding to Figures 4a – c. For all cases, the energy of both crystals show less than 1% deviation from its initial value, indicating the stability and energy conservation of the MI process. However, for the case of Q_U at higher crystal temperature, the energy fluctuation is relatively less, while for the case of $Q_{\hat{U}}$ it is reversed. The peak in Q_U for $\hat{T} = 340$ K at $\xi \approx 3.8$, as shown in Figure 6a, for an example, is due to the interact of breathers, as depicted in Figure 4c.

4. Conclusions

In this paper, we have derived analytic expressions for the MI gain in a photovoltaic photorefractive crystal circuit modeled by (1). The dependence of the temperature of crystal $\hat{P}$, the photovoltaic filed $E_{\rm p}$, and the power R on the gain was demonstrated in Figure 1. It has been found that any initial perturbation can be unstable since the MI gain is non-zero for modulation frequency other than $\Omega = 0$ regardless of the parameters of the crystals. We have investigated the effects of the crystal temperature on the evolution of the initial localized beams in Figures 2a – c, which transform into the breather and the stable stationary solitary wave. We found in Figure 3 that the localized beams induced from the perturbed CW states under the MI transform into the various transient wave structures which interact to form the symmetric and asymmetric solitary-waves, as shown in Figure 3c. In particular, it has been demonstrated that the energy variation during the MI process is very small. The effects of the crystal temperature on the perturbed CW states under the MI have been demonstrated in Figures 4a – c for different temperatures. It was shown that the coherent structure formation by the MI process is quite sensitive to the crystal temperature. The highly periodic and symmetric waves were shown to exist regardless of the crystal temperature as demonstrated in Figures 5a – b. It has been found in Figures 6a – b that the energy of both crystals shows less than 1% deviation from its initial value, indicating the stability and energy conservation of the MI process.

Acknowledgement

This work was supported by Catholic University of Daegu in 2009.

[1] Y. S. Kivshar and G. P. Agrawal, Optical Solitons: From Fibers to Photonic Crystals, Academic Press, San Diego, California 2003.
[2] S. Trillo and W. Torruellas (ed.), Spatial Solitons, Springer, Berlin 2001.
[3] D. Mihalache, D. Mazilu, I. Towers, B. A. Malomed, and F. Lederer, Phys. Rev. E **67**, 056608 (2003).
[4] S. Konar and A. Sengupta, J. Opt. Soc. Am. B **11**, 1644 (1994).
[5] G. P. Agrawal, Nonlinear Fiber Optics, Academic Press, Boston, MA 1995.
[6] G. Duree, J. L. Slultz, G. Salamo, M. Segev, A. Yariv, B. Crosignani, P. DiPorto, E. Sharp, and R. R. Neurgaonkar, Phys. Rev. Lett. **71**, 533 (1993).
[7] M. Segev, B. Crosignani, A. Yariv, and B. Fischer, Phys. Rev. Lett. **68**, 923 (1992).
[8] M. F. Shih, M. Segev, G. C. Valley, G. J. Salamo, B. Crosignani, and P. DiPorto, Electron. Lett. **31**, 826 (1995).
[9] G. Couton, H. Maillotte, and M. Chauvet, J. Opt. B, Quantum Semiclass. Opt. **6**, 223 (2004).
[10] S. Lan, J. A. Giordmaine, M. Segev, and D. Rytz, Opt. Lett. **27**, 737 (2002).
[11] M. Chauvet, S. A. Hawkins, G. Salamo, M. Segev, D. F. Bliss, and G. Bryant, Appl. Phys. Lett. **70**, 2499 (1997).

[12] L. Jinsong and L. Keqing, J. Opt. Soc. Am. B **16**, 550 (1999).
[13] J. Liu and Z. Hao, J. Opt. Soc. Am. B **19**, 513 (2002).
[14] L. Keqing, T. Tiantong, and Z. Yanpeng, Phys. Rev. A **61**, 053822 (2000).
[15] C. Hou, Y. Zhang, Y. Jiang, and Y. Pei, Opt. Comm. **273**, 544 (2007).
[16] W. P. Hong, Opt. Com. **213**, 173 (2002).
[17] W. P. Hong, Z. Naturforsch. **61a**, 225 (2006).
[18] H. Leblond and C. Cambournac, J. Opt. A, Pure Appl. Opt. **6**, 461 (2004).
[19] S. K. Nam and J. Yi, J. Korean Phys. Soc. **47**, 1041 (2005).
[20] G. Zhang, J. Liu, C. Wang, H. Zhang, and S. Liu, J. of Mod. Optics **54**, No. 4, 579 (2007).
[21] L. Cheng and A. Partovi, Appl. Phys. Lett. **49**, 1456 (1986).
[22] Z. Guangyong, L. Jinsong, W. Cheng, Z. Huilana, and L. Shixiong, Optik **119**, 303 (2008).
[23] J. A. C. Heideman and B. M. Herbst, SIAM J. Numer. Anal. **23**, 485 (1986).